ORIGINAL RESEARCH

Interaction and mechanism of nitrocellulose and *N*-methyl-4-nitroaniline by isothermal decomposition method

Liqiong Luo · Bo Jin · Zuohu Chai · Qiong Huang · Shijin Chu · Rufang Peng

Abstract The influence of *N*-methyl-4-nitroaniline (MNA) on the thermal stability of nitrocellulose (NC) was investigated via an isothermal decomposition dynamics research method. The Arrhenius equation and model-fitting were used to calculate the thermal decomposition kinetic parameters of NC and MNA/ NC (3 wt%) composite. Results showed that the thermal decomposition activation energy of NC/MNA (3 wt%) was significantly increased compared with that of pure NC, indicating that the thermal stability of NC was increased with stabilizer MNA addition. Subsequently, the storage life of NC and MNA/NC (3 wt%) composite was estimated using Berthelot equation. It was found that if the decomposition extent reaches 0.1% as the end of life criterion, 3 wt% stabilizer MNA addition significantly extended the storage life of NC from 10.57 to 24.9 years at ambient temperature (298.15 K) with the life extension rate reaching 135.6%. Furthermore, the intermediate product produced by MNA and NC action was extracted and characterized via UV–Vis, HPLC, ^{1}H NMR, FT-IR, and LC–MS, and a possible stabilization mechanism of MNA to NC was proposed.

Keywords Nitrocellulose · *N*-methyl-4-nitroaniline · Stabilizer · Isothermal decomposition · Storage life

L. Luo · B. Jin (✉) · Z. Chai · Q. Huang ·
S. Chu · R. Peng (✉)
State Key Laboratory of Environment-friendly Energy Materials, Southwest University of Science and Technology, Mianyang 621010, Sichuan, China
e-mail: jinbo0428@163.com

R. Peng
e-mail: rfpeng2006@163.com

Introduction

Nitrocellulose (NC) is a highly flammable polymer formed by nitrating cellulose via exposure to nitric acid or another powerful nitrating agent; NC has been widely employed in various military and civilian applications (Tan 2015; Chai et al. 2019; Cui et al. 2001; Tai et al. 2018). Among them, the military application of NC is mainly concentrated in the field of propellants and explosives, serving as the main component of solid propellants, gun propellants, and some mixed explosives (Trache and Tarchoun 2018a, b). Given that NC structure contains a large number of nitrate groups that are inherently chemically unstable due to autocatalytic accelerated decomposition, NC has short storage and service life, poor ballistic performance, and the possibility to self-combust or become an explosive safety hazard (Zayed et al. 2000, 2010, 2012, 2013; Zayed and Hassan 2010; Lin et al. 2016; Trache and Khimeche 2013a, b). The

autocatalytic accelerated decomposition of nitrates is attributed to their decomposition products, including nitrogen oxides and nitric acids that can catalyze decomposition (Frys et al. 2011; Trache et al. 2013a, b). Therefore, to inhibit the autocatalytic decomposition of nitrates and improve their stability, some alkalescent chemical stabilizers are usually added in nitrate-based energetic materials (Trache et al. 2013a, b). The stabilizers mostly cannot prevent nitrate ester decomposition but are able to inhibit this process, effectively preventing the catalytic effect caused by the decomposition products, such as NO, NO_2, HNO_2 and HNO_3 (Lindblom 2002; Boers 2010). Numerous stabilizers have been reported, such as aniline, urea, and phenol ether stabilizers (Lussier et al. 2006; Wilker et al. 2007; Krumlinde et al. 2017). Nevertheless, considerable effort in recent years has been devoted to the development of new stabilizers. Only a few reports on the interactions and mechanisms between stabilizers and nitrate esters are available mainly because of limited research methods.

Traditional stabilizer evaluation methods, such as Wiley test, methyl violet test, and Abel test, require observation with the naked eye to determine the time required for color change, thereby associated with highly subjective factors with action process and mechanism that cannot be studied (Trache and Tarchoun 2018a). Several non-isothermal decomposition research methods, such as thermogravimetric method and differential scanning calorimetry methods, can determine limited decomposition kinetic parameters, but they are based on rapid heating and cannot reflect slow NC decomposition. In contrast, isothermal decomposition can reflect the actual decomposition situation perfectly, by virtue of their relatively low temperature, large sample consumption, small weighing error, the homogeneous and representative sample, and facilitates determination of slow chemical reactions. Unfortunately, accelerated aging test is a common isothermal decomposition method to predict the storage life without continuous monitoring (Zhao et al. 2018). Bergmann–Junk (BJ) and Vacuum Stability Test (VST) were applied to investigate the effect of organic eutectic mixture on the stability of NC even though they have complex operation, many steps, and high labor cost (Chelouche et al. 2019). In our previous work, a new isothermal decomposition dynamics research instrument has been developed to effectively circumvent these challenges and has been

successfully applied to study CL-20 and NC isothermal decomposition kinetics (Luo et al. 2019a, b; Xiao et al. 2016). To continue our interest in isothermal decomposition, we used this instrument to study the interaction and mechanism of NC and stabilizers. Considering the currently reported stabilizers, strikingly, N-methyl-4-nitroaniline (MNA) is an attractive candidate for NC stabilization because of its appealing capability to retain the nitrogen oxides, good thermal stability, and facile synthesis from abundant and inexpensive starting materials (Trache et al. 2018; Tang et al. 2016). Herein, we first studied the isothermal kinetics and interaction mechanisms between NC and MNA by using the isothermal thermal decomposition device, and the effect of MNA on the storage life of NC was estimated using Berthelot equation. Intermediate product structure resulting from MNA and NC action was further confirmed using UV–Vis, HPLC, FT-IR, LC–MS, and ^{1}H NMR, and the possible stability mechanism of MNA to NC was proposed.

Experimental

Materials

MNA (purity > 99%), ethyl alcohol, acetonitrile, and dichloromethane were of analytical grade. All of the above chemicals were purchased from Kelong Chemical Reagents Company (Chengdu, China) and used without further purification. NC with 12.76% nitrogen content was supplied by the China Academy of Engineering Physics (Mianyang, Sichuan). Deionized water used in HPLC was from local sources.

Caution! NC is an explosive hazardous with sensitivity to various stimuli. During storage, fire and static electricity discharge should be avoided and the storage temperature don't exceed 313.15 K. For security, wetting agent such as water and ethanol should be added. When experimenting, metal spatulas are strictly forbidden. Once the pressure rises too fast in the experiment, the experiment should be stopped immediately. Extreme caution is advised.

Preparation

NC/MNA (3 wt%) composites were well combined via the simple solvent evaporation method. The

selected weight addition ratio of MNA was 3 wt% (Chelouche et al. 2019). Briefly, a total of 92.8 mg of MNA was dissolved in 10 mL of ethanol under ultrasonic conditions to obtain a solution of 9.28 mg/mL of MNA in ethanol. Then, 1.0 mL of above-mentioned solution was added to a test tube containing 300 mg of NC, which was uniformly dispersed on the NC surface under ultrasonic conditions. Thereafter, the mixtures were dried at 323.15 K under vacuum condition until constant weight to obtain the NC/MNA (3 wt%) composites.

After the isothermal decomposition of NC/MNA (3 wt%) reached a certain reaction extent, 20 mL of dichloromethane was added to extract the residue under ultrasonic conditions. The extraction was repeated several times until there was no product was left, and the filtrates were combined for further analytical testing.

Instruments and methods

The isothermal decomposition of NC/MNA (3 wt%) was determined using an isothermal decomposition dynamics research instrument (Luo et al. 2019a, b). The instrument is composed of pressure sensor, thermostat, pressure transmitter, DC power supply, computer, vacuum pump, and some fittings (Fig. 1 and Fig. S1†). Samples (300 mg) were investigated isothermally at different temperatures (i.e., 378.15 K, 383.15 K, 388.15 K, 393.15 K and 398.15 K). To obtain the total gas pressure of NC/MNA (3 wt%), 10 mg NC/MNA (3 wt%) was completely decomposed at 433.15 K. Thermal

reaction units with samples were sealed tightly and evacuated to the initial pressure below 0.1 kPa, and pressure values were kept stable over 24 h to ensure that they were sealed well. After setting the heating program of the temperature controller, the reaction units were heated from room temperature to the target temperature with a constant heating rate (2 K/min) and consistently maintained at the target temperature isothermally unremittingly. They were placed into the constant temperature thermostat, and data-collection interval was 1 min.

Characterization

Ultraviolet–visible (UV–Vis) spectra were performed a UV-1600 spectrophotometer with acetonitrile as the solution. Elite high performance liquid chromatography (HPLC) P230 was used for analysis. The separation was done on a UV detector, and sampling was done with an auto sampler. Data collection for chromatogram was done by N2000. The column used was Welchrom-C18 (250 mm × 4.6 mm) with mobile phase of acetonitrile–water (the ratios of volume = 60:40) mixture solvent. Filtration of mobile phase was carried out by 0.45 μm membrane filter under the isocratic condition with flow rate of 0.5 mL min^{-1}, injected volume of 20 μL, and elution monitored at 345 nm with run time of 15 min. Fourier transform infrared spectroscopy (FT-IR) was recorded with a Nicolet-5700 FT-IR spectrometer using pressed KBr pellet in the range of 4000–400 cm^{-1}. ^{1}H NMR spectra of the intermediate product produced by the action of MNA and NC was collected using a JEOL
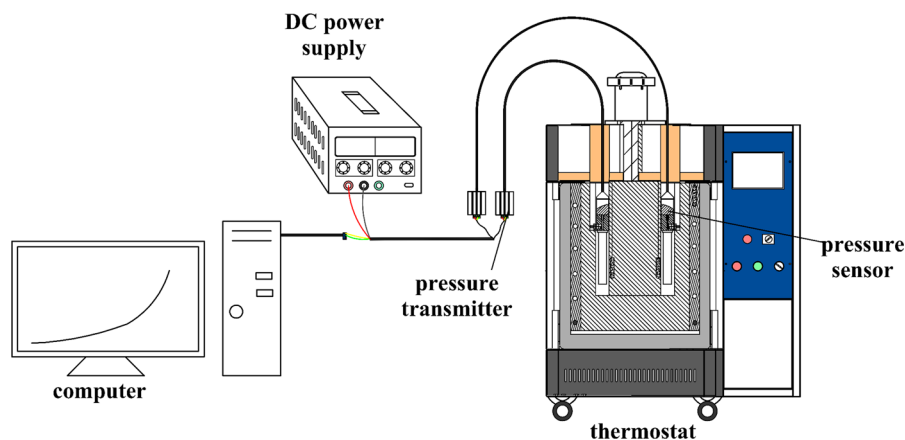

Fig. 1 Schematic of components connecting the isothermal decomposition dynamics research instrument
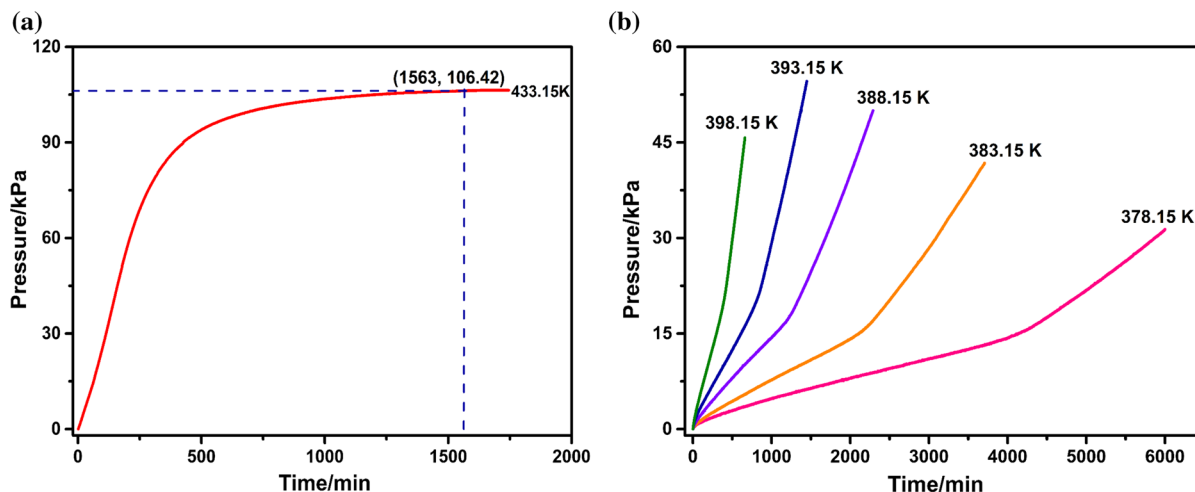
Fig. 2 Time dependence of the standardized gas pressure of NC/MNA (3 wt%) under the unified temperature of 298.15 K: **a** complete decomposition at 433.15 K; **b** at different temperatures of 378.15 K, 383.15 K, 388.15 K, 393.15 K, and 398.15 K

GSX 400-MHz nuclear magnetic resonance (NMR) spectrometer in CDCl$_3$ solution. Liquid chromatography–mass spectrometry (LC–MS) was a varian equipped with an electrospray ionization (ESI), source using negative mode.

Results and discussion

Isothermal thermal decomposition and stability of NC and NC/MNA (3 wt%)

The sample was measured isothermally at 378.15 K, 383.15 K, 388.15 K, 393.15 K, and 398.15 K using an isothermal decomposition dynamics research instrument. Then, the pressure values were converted into standardized pressure values under the unified temperature of 298.15 K in accordance with the equation as follows (Luo et al. 2019a, b; Xiao et al. 2016):

$$\frac{P_1}{P_0} = \frac{T_1}{T_0} \qquad (1)$$

where P_1 is the net pressure values (kPa), T_1 is the corresponding test temperature (K), P_0 is the standardized net pressure values (hereafter referred to as pressure values), and T_0 is 298.15 K.

The standardized gas pressure–time curves of NC/MNA (3 wt%) under 298.15 K are depicted in Fig. 2.

Thermal decomposition of 10 mg NC/MNA (3 wt%) at 433.15 K from the acceleration period to the constant velocity and deceleration period is clearly illustrated (Fig. 2a). With NC/MNA (3 wt%) decomposition, pressure gradually increased over time until it remained constant, indicating that decomposition was complete. At 433.15 K, the time observed to complete the conversion of 10 mg NC/MNA (3 wt%) was 1563 min, and the total gas pressure was 106.42 kPa, suggesting that 3192.45 kPa was the gas pressure produced by the complete decomposition of 300 mg samples. Figure 2b shows the pressure–time curves of NC/MNA (3 wt%) at different temperatures. All pressure–time curves obtained via the isothermal decomposition of NC/MNA (3 wt%) at 378.15 K, 383.15 K, 388.15 K, 393.15 K and 398.15 K had a significant inflection point. Notably, compared with the pressure–time curve of pure NC at the same temperature, the pressure of the gas generated by NC/MNA (3 wt%) decomposition before the inflection point was remarkably slower with time (Fig. 3). Subsequently, the pressure increase rate of NC/MNA (3 wt%) decomposition increased rapidly after the inflection point, which is attributed to the stabilizer MNA was consumed. The autocatalytic decomposition of nitrogen oxides generated by NC decomposition further accelerated NC/MNA decomposition.
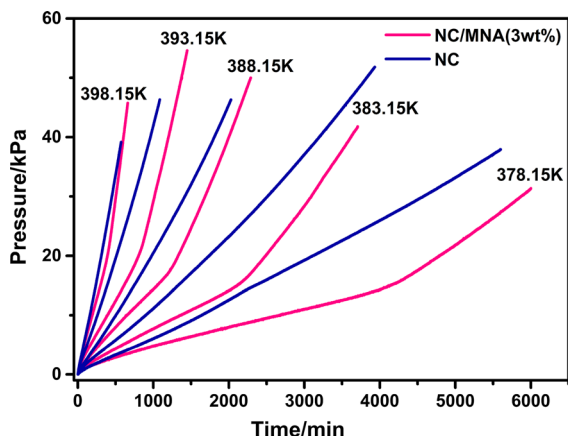
Fig. 3 Comparison curve of pressure–time of NC and NC/MNA (3 wt%) under the unified temperature of 298.15 K

Effect of stabilizer MNA on the isothermal decomposition kinetics of NC

The isothermal decomposition process was investigated to explore the stabilizer (MNA) effect on isothermal decomposition kinetics of NC. The isothermal decomposition kinetics was calculated using both Arrhenius equation and the model-fitting method (Hu et al. 2008). The kinetic parameters of solid-state reaction, including activation energy (E_a), pre-exponential factor (A), mechanism model G(α), and reaction rate constant k should be determined for a complete kinetic description.

The extent of reaction (α) is defined as follows (Hu et al. 2008; Liu et al. 2012):

$$\alpha = \frac{P}{P_T} \qquad (2)$$

where P (kPa) is the pressure of the gas generated by NC or NC/MNA (3 wt%) decomposition at any time and P_T (kPa) denotes total gas pressure produced by complete decomposition of NC or NC/MNA (3 wt%). According to the gas pressure data generated by NC/MNA (3 wt%) decomposition under different isothermal conditions with time, the time required for different decomposition extents of NC/MNA (3 wt%) can be calculated using Eq. (2). Figure 4 schematically displays the corresponding pressure and time of NC/MNA (3 wt%) at different decomposition extent. Obviously, the decomposition depth of the NC/MNA (3 wt%) isothermal decomposition pressure–time curve inflection point was between 0.5
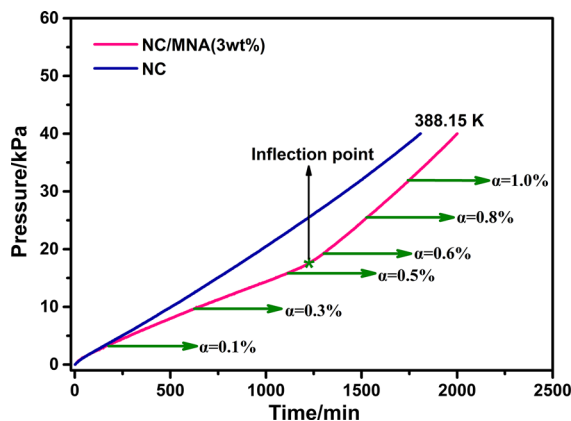

Fig. 4 Corresponding pressure and time of NC/MNA (3 wt%) at different decomposition degrees under 388.15 K isothermal decomposition conditions

and 0.6. Table 1 exhibits the time required for NC/MNA (3 wt%) decomposition to attain a certain extent at different temperatures, wherein, the decomposition depth $\alpha = 0.1$–0.5% corresponds to "before inflection point" and $\alpha = 0.6$–1.0% corresponds to "after inflection point."

Arrhenius equation was as follows (Chu 1994; Hu et al. 2008):

$$\log t = -\log A + E_a/2.303RT \qquad (3)$$

where t is the time required to attain a certain decomposition extent (s), A denotes the pre-exponential factor (s^{-1}), E_a represents the decomposition activation energy (kJ mol^{-1}), R stands for the gas constant (8.314 kJ K^{-1} mol^{-1}), and T indicates the isothermal decomposition temperature (K). Data in Table 1 were computed using Eq. 3, and log$t$ was plotted against T^{-1} (Fig. 5). Corresponding apparent activation energy E_a and pre-exponential factor A of NC/MNA (3 wt%) under different decomposition extents can be calculated from the slope and intercept. Similarly, the apparent activation energy E_a and pre-exponential factor A of NC under different decomposition extents can be calculated according to Arrhenius equation. As shown in Table 2, the decomposition activation energies of pure NC at decomposition extents of 0.5% and 1.0% were similar at 145.6 kJ mol^{-1} and 146.3 kJ mol^{-1}, respectively, implying that NC decomposition mechanism at different decomposition extents is consistent. However, the NC/MNA (3 wt%) decomposition activation energy before and after the inflection point was very

Table 1 Time required for NC/MNA (3 wt%) to attain a certain decomposition depth extent at different isothermal decomposition temperatures

Decomposition extent (α) (%)	378.15 K t/min	383.15 K t/min	388.15 K t/min	393.15 K t/min	398.15 K t/min
0.1	573	330	162	90	48
0.2	1494	800	385	228	114
0.3	2527	1290	618	373	183
0.4	3577	1805	870	516	251
0.5	4302	2206	1122	653	319
0.6	4686	2432	1297	777	379
0.7	5062	2632	1418	869	424
0.8	5411	2829	1531	931	459
0.9	5746	3020	1642	992	491
1.0	6060	3228	1748	1051	525
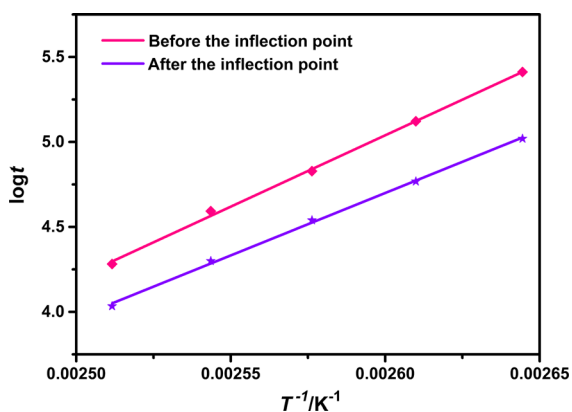
Fig. 5 Plot of log$t$ versus T^{-1} of NC/MNA (3 wt%)

different. In detail, before the inflection point, the activation energy at a decomposition depth of 0.5% was 160.8 kJ mol^{-1}, and the activation energy at a decomposition depth of 1.0% after the inflection point was 140.7 kJ mol^{-1}. The decomposition activation energy of NC/MNA (3 wt%) before the inflection point was significantly higher than that of NC, which manifests that NC was increasingly stabilized with MNA addition. The decomposition activation energy of NC/MNA (3 wt%) after the inflection point was

slightly lower than that of NC, which should be caused by the consumed stabilizer MNA in the NC/MNA (3 wt%) as decomposition progressed further.

Additionally, the model-fitting method was also used to study the isothermal decomposition kinetics of NC/MNA (3 wt%). The most probable reaction mechanism was selected from 41 kinds of commonly used mechanisms by the least square method based on the model fitting principle, which is the basis of the fitting line with the maximum correlation coefficient and the minimum intercept. The model-fitting method equation is as follows (Hu et al. 2008):

$$G(\alpha) = kt \tag{4}$$

before the inflection point, data with 0.1%, 0.2%, 0.3%, 0.4%, and 0.5% decomposition extents were selected for calculation. After the inflection point, the data with 0.6%, 0.7%, 0.8%, 0.9%, and 1.0% decomposition extents were selected for calculation. Through the G(α) versus t relationship of linear regression before and after the inflection point, best mechanism functions and kinetics parameters under different temperatures were obtained, as depicted in Tables 3 and 4. For NC/MNA (3 wt%), at 378.15–398.15 K, the models consistently conformed to No.28, corresponding to the reaction order (n = 1/4)

Table 2 Kinetic parameters of NC/MNA (3 wt%) and NC based on Arrhenius equation

| Sample	Decomposition extent (α)	E_a (kJ mol^{-1})	log$A$	R
NC/MNA (3 wt%)	0.5% (before the inflection point)	160.8	16.79	0.9980
	1.0% (after the inflection point)	140.7	14.40	0.9983
NC	0.5%	145.6	14.91	0.9986
	1.0%	146.3	14.73	0.9990

Table 3 Decomposition reaction constant rate and mechanism function of NC/MNA (3 wt%) before the inflection point via model-fitting method

Temperature (K)	Model no.	Model name	$k \times 10^{-9}$ s^{-1}	G(α)	R
378.15	28	Reaction order n = 1/4	4.36	$1 - (1 - \alpha)^{1/4}$	0.9956
383.15	28	Reaction order n = 1/4	8.77	$1 - (1 - \alpha)^{1/4}$	0.9982
388.15	28	Reaction order n = 1/4	17.35	$1 - (1 - \alpha)^{1/4}$	0.9990
393.15	28	Reaction order n = 1/4	29.53	$1 - (1 - \alpha)^{1/4}$	0.9999
398.15	28	Reaction order n = 1/4	61.50	$1 - (1 - \alpha)^{1/4}$	0.9999

Table 4 Decomposition reaction constant rate and mechanism function of NC/MNA (3 wt%) after the inflection point via model-fitting method

Temperature (K)	Model no.	Model name	$k \times 10^{-8}$ s^{-1}	G(α)	R
378.15	28	Reaction order n = 1/4	1.23	$1 - (1 - \alpha)^{1/4}$	0.9985
383.15	28	Reaction order n = 1/4	2.20	$1 - (1 - \alpha)^{1/4}$	0.9984
388.15	28	Reaction order n = 1/4	3.79	$1 - (1 - \alpha)^{1/4}$	0.9994
393.15	28	Reaction order n = 1/4	6.87	$1 - (1 - \alpha)^{1/4}$	0.9999
398.15	28	Reaction order n = 1/4	12.54	$1 - (1 - \alpha)^{1/4}$	0.9999

either before or after the inflection point, which agrees fairly well with pure NC. Hence, MNA addition did not change the mechanism function of NC. Furthermore, compared with that of pure NC, the k value before the inflection point was smaller while the k value after the inflection point was larger (Fig. 6), suggesting that NC/MNA (3 wt%) decomposition was slower before the inflection point. As decomposition
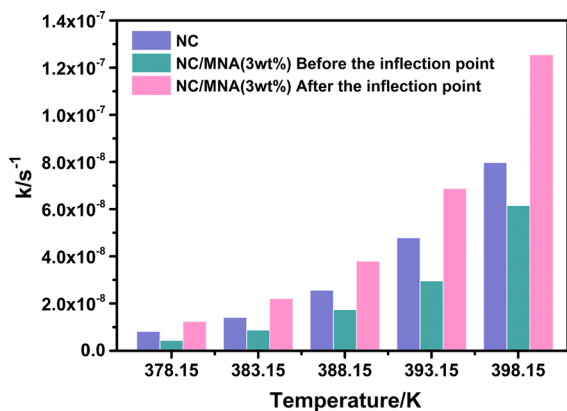
Fig. 6 Comparison histogram of reaction rate-temperature of NC and NC/MNA (3 wt%)

progressed, the stabilizer MNA was consumed, and NC/MNA (3 wt%) decomposition increased sharply after the inflection point.

Afterward, the Arrhenius parameters were evaluated via the Arrhenius equation:

$$\ln k = -E_a/RT + \ln A \tag{5}$$

where k is the reaction rate constant (s^{-1}), E_a represents the activation energy (kJ mol^{-1}), R denotes the gas constant (8.314 kJ K^{-1} mol^{-1}), T indicates the temperature (K), and A refers to the pre-exponential factor (s^{-1}). When ln$k$ was plotted against T^{-1}, two straight lines approximately before and after the inflection point were obtained through linear fitting (Fig. 7). The experimental points before the inflection point were described as ln$k = -$ 19,592.86/T + 32.57 with $R = 0.9974$, and the experimental points after the inflection point followed ln$k = -$ 17,398.13/T + 27.77 with $R = 0.9987$. According to the slope and intercept of abovementioned equations based on the model-fitting method, the isothermal thermal decomposition kinetic parameters of NC/MNA (3 wt%) before and after the inflection point are listed in Table 5. As such, the isothermal decomposition activation energy of NC/MNA (3 wt%) before the
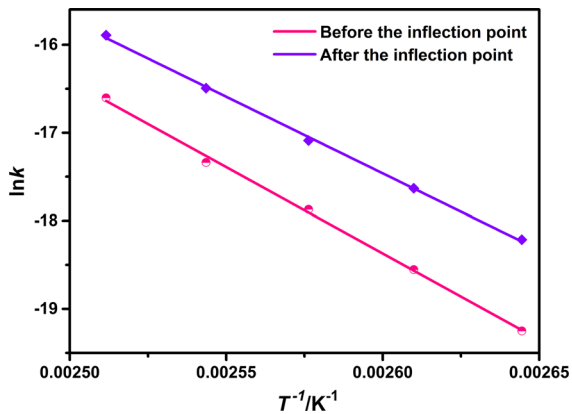
Fig. 7 Plot of ln$k$ versus T^{-1} of NC/MNA (3 wt%)

inflection point was significantly higher than that of NC, and the isothermal decomposition activation energy of NC/MNA (3 wt%) after the inflection point was slightly lower than that of NC.

To get insight into the effect of MNA content on NC isothermal decomposition, we conducted the thermal decomposition of NC/MNA (1 wt%), NC/

MNA (2 wt%), NC/MNA (3 wt%), NC/MNA (4 wt%), and NC/MNA (5 wt%) at 388.15 K. Figure 8a displays the pressure–time curves of NC/MNA with different MNA content. It was found that increased MNA content in NC/MNA prolonged the time for the pressure–time curve of NC/MNA to reach the inflection point and the degree of thermal decomposition (α), corresponding to the inflection point increase (Fig. 8b). Previous results have shown that NC/MNA isothermal decomposition before the inflection point was slower than that of NC. Above results readily elucidate that the NC/MNA became increasingly stable as the MNA content in the NC/MNA increased.

Effect of stabilizer MNA on NC storage life

Berthelot equation (Zhao et al. 2018; Hu et al. 2008) is suitable for a consistent G(α) with the same decomposition extent at different temperatures and applied to calculate the storage life, as follows:

$$\log t_T = a + b \times T \tag{6}$$

Table 5 Kinetic parameters of NC/MNA (3 wt%) and NC based on the model fitting method

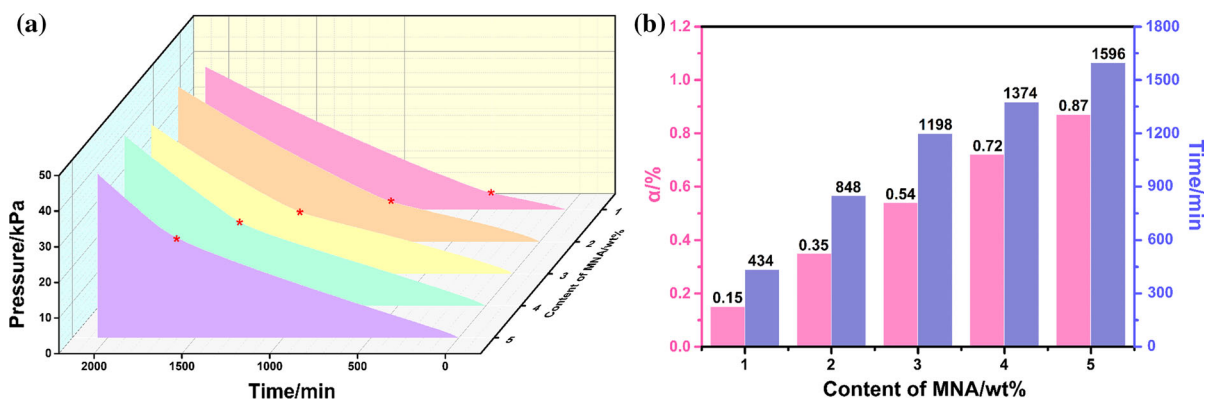| Sample	Decomposition extent (α)	E_a (kJ mol^{-1})	ln$A$	R
NC/MNA (3 wt%)	0.1–0.5% (before the inflection point)	162.9	32.57	0.9974
NC/MNA (3 wt%)	0.6–1.0% (after the inflection point)	144.6	27.77	0.9987
NC	0.1–0.5%	144.7	27.39	0.9986

Fig. 8 **a** Pressure–time curves of NC/MNA with different MNA content at 388.25 K: NC/MNA (1 wt%), NC/MNA (2 wt%), NC/MNA (3 wt%), NC/MNA (4 wt%), and NC/MNA (5 wt%); **b** the histogram of decomposition extent (α) and time with

different MNA content at 388.25 K: NC/MNA (1 wt%), NC/MNA (2 wt%), NC/MNA (3 wt%), NC/MNA (4 wt%), and NC/MNA (5 wt%)
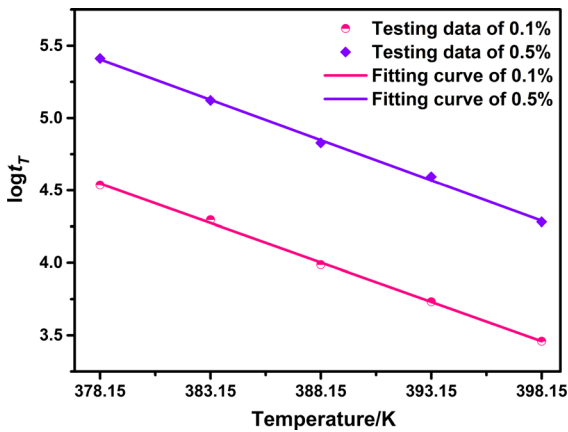
Fig. 9 Plot of $\log t_T$ against T of NC/MNA (3 wt%)

where t_T is the reaction time to reach a certain extent of reaction, a and b denote the undetermined coefficients, and T is the temperature for calculated. Data in Table 1 were calculated using Eq. 6, and $\log t_T$ was plotted against T (Fig. 9). The corresponding life equations under different decomposition depth conditions were obtained (Table 6). Then, the storage lives of NC and

NC/MNA (3 wt%) at 298.15 K, 323.15 K, 343.15 K, 363.15 K, and 378.15 K were estimated using the obtained life equations. As shown in Table 6, if the time required for the decomposition extent (α) reached 0.1% as the end of life, the effective storage life of NC at ambient temperature (298.15 K) was 10.54 years. The effective storage life of NC/MNA (3 wt%) was 24.94 years, revealing that addition of 3% stabilizer MNA extended the life of NC by 136.5%. If the time required for the decomposition extent (α) to reach 0.5% as the end of life was used, NC/MNA (3 wt%) lifespan at 298.15 K was 233.06 years, which is about 340% longer than that of NC.

Additionally, for comparison, Arrhenius–Van't Hoff equation (Shekhar 2011) is also used to predict storage life. It was given by Eq. (7):

$$\frac{t_2}{t_1} = (\gamma_{10})^{\frac{T_1-T_2}{10}} \tag{7}$$

where t_2 is storage life at temperature T_2, t_1 is storage life at temperature T_1. And 10 °C is taken as a standard and for every 10 °C rise or fall in temperature, the sample properties changes by the same fraction,

Table 6 The estimated time of NC/MNA (3 wt%) and NC to reach a certain decomposition extent at various temperatures based on Berthelot equation and Arrhenius–Van't Hoff equation

| Sample	α (%)	Method	Empirical formulas	R	Time (years) 298.15 K	Time (years) 323.15 K	Time (days) 343.15 K	Time (days) 363.15 K	Time (min) 378.15 K
NC	0.1	Berthelot equation	$\log t_T = -0.0509T + 23.70$	0.9903	10.57	0.56	19.71	1.89	469
NC	0.5	Berthelot equation	$\log t_T = -0.0505T + 24.28$	0.9984	52.91	2.89	103.12	10.08	2536
NC/ MNA (3 wt%)	0.1	Berthelot equation	$\log t_T = -0.0544T + 25.10$	0.9985	24.94	1.09	32.58	2.67	587
NC/ MNA (3 wt%)	0.5	Berthelot equation	$\log t_T = -0.0558T + 26.49$	0.9981	233.06	9.40	263.09	20.17	4232
NC/ MNA (3 wt%)	0.1	Arrhenius– Van't Hoff equation	–	–	24.55	1.07	31.92	2.61	573
NC/ MNA (3 wt%)	0.5	Arrhenius- Van't Hoff equation	–	–	246.76	9.83	272.26	20.66	4302
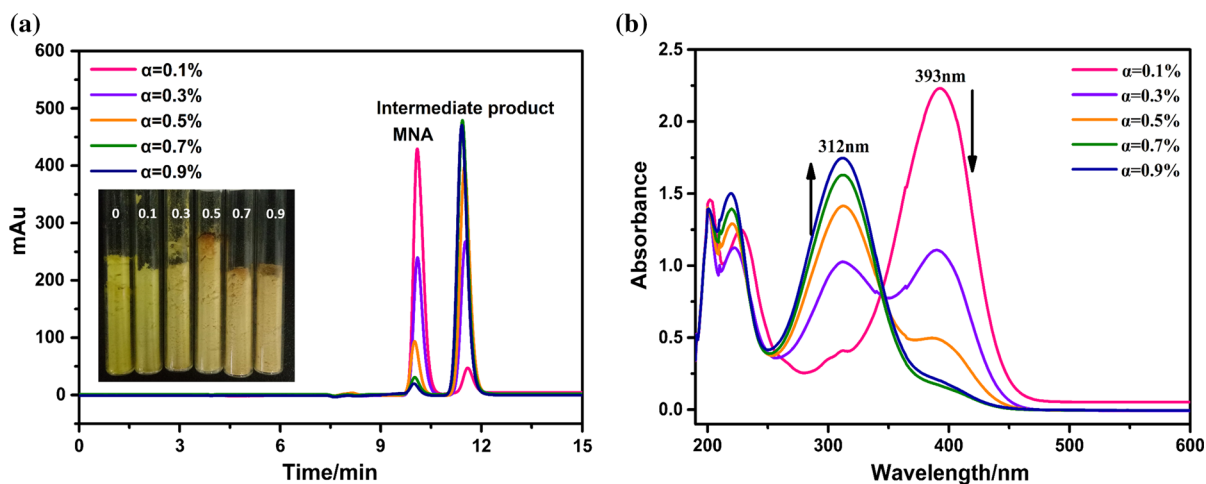
Fig. 10 a HPLC chromatograms of decomposition residues of NC/MNA (3 wt%) with different degrees of decomposition; inset: image showing the different decomposition extents of NC/

MNA (3 wt%); b UV–Vis spectra of different decomposition extents of NC/MNA (3 wt%)

Table 7 Consumption percentage of MNA in NC/MNA (3 wt%) at different decomposition extents

Decomposition extent (α)	0	0.1%	0.3%	0.5%	0.7%	0.9%
Consumption percentage of MNA (%)	0	17	58	85	96	97

defined by γ_{10}. The storage lives of NC and NC/MNA (3 wt%) at 298.15 K, 323.15 K, 343.15 K, 363.15 K, and 378.15 K were estimated according to Eq. (7) and also listed in Table 6. Results show that the estimated storage lives from the two methods are almost the same. These results disclosed that the addition of stabilizer MNA can significantly improve the thermal stability of NC and prolong its storage life.

Stability mechanism of stabilizer MNA to NC

To obtain the intermediate product information produced by MNA and NC action and confirm the interaction mechanism of MNA on NC stability, NC/MNA residues with different decomposition extents ($\alpha = 0.1\%$, 0.3%, 0.5%, 0.7%, and 0.9%) were conducted by HPLC and UV–Vis spectroscopy. HPLC chromatograms of NC/MNA (3 wt%) decomposition residues with different decomposition extents are showed in Fig. 10a. With the increase of the decomposition extent of NC/MNA (3 wt%), the MNA content decreased gradually at 10.09 min, and a new intermediate appeared at 11.44 min. The intermediate

content increased with the increase of NC/MNA (3 wt%) decomposition extent. The UV–Vis results were consistent with that of HPLC. As shown in Fig. 10b and Fig. S2†, MNA (393 nm) content was significantly reduced, while a new absorption peak appeared at 312 nm as the decomposition extent of NC/MNA (3 wt%) increased, deeming that MNA was converted as an intermediate product. The MNA content in the NC/MNA residue at different decomposition extent was further quantified using HPLC (Fig. S3† and Table 7). It can be inferred that the MNA consumption percentage was greater than 90% when the degree of conversion was greater than 0.6%. Thus, MNA was almost consumed when the NC/MNA (3 wt%) thermal decomposition pressure–time curve reached the inflection point, which is consistent with the previous isothermal decomposition kinetics results. The MNA consumption followed the first-order kinetics, as seen in the linear fitting profiles shown in Fig. S4†. The first-order rate constant (k) was calculated using the equation, as follows:
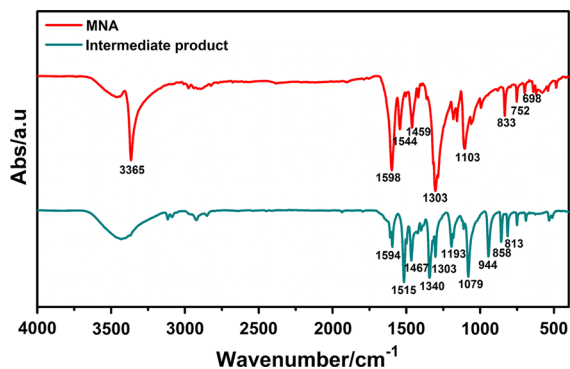
$$-\ln(C_t/C_0) = kt \qquad (8)$$

Fig. 11 FT-IR spectra of raw MNA and intermediate product obtained from the NC/MNA (3 wt%) isothermal decomposition residue

where C_0 and C_t are the MNA compound concentration at the isothermal decomposition time of 0 and t, respectively. The calculated kinetic rate constant k was 0.0027 min^{-1} with the correlation coefficients of approximately 0.9679.

To further confirm the molecular structure of the intermediate product produced by MNA and NC action, FT-IR, ^{1}H NMR, and LC–MS were carried out. The characteristic bands in the FT-IR spectrum of MNA and the intermediate product are shown in Fig. 11. The IR spectrum of the intermediate product

showed that N–H stretching vibration characteristic peak was not observed in 3365 cm^{-1} region, whereas it was observed in the IR spectrum of MNA. Strong absorption at 1515 cm^{-1} in the IR spectrum was assigned to the nitroso group. As shown in Fig. 12, the ^{1}H NMR spectrum of the intermediate product illustrated two double peaks of the para-substituted benzene ring in the benzene ring region, explaining that MNA benzene ring did not participate in the reaction. N–H proton signal was absent between 5 and 6 ppm, whereas methyl proton signal was found at 3.4 ppm because the anisotropic deshielding effect of the nitroso group shifted the position of the methyl proton to a high ppm. The ^{1}H NMR spectrum clearly exhibited that the intermediate product after MNA and NC action has lost the hydrogen on the nitrogen. Above results manifested that the intermediate product produced by the action of MNA and NC was N-methyl-N-(4-nitrophenyl) nitrous amide (N-NO-MNA). Then, LC–MS was also performed to give direct proofs for the intermediate product structure, and its mass spectrum demonstrated a molecular ion peak at m/z = 180.8, which is consistent with that of a nitroso group in place of the hydrogen in N–H (Fig. S5†). The intermediate product structure resulting from the action of MNA and NC was also in
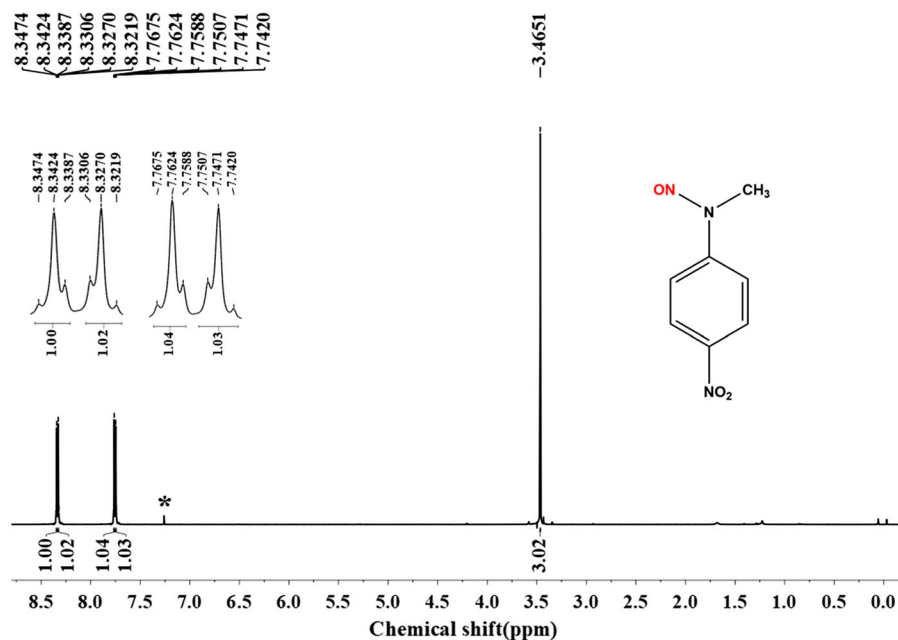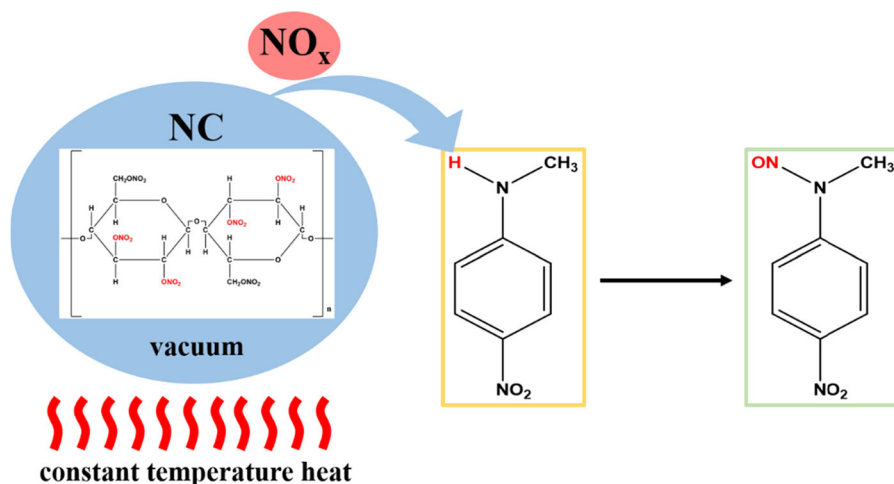

Fig. 12 ^{1}H NMR of intermediate product obtained from the NC/MNA (3 wt%) isothermal decomposition residue

Fig. 13 Potential stabilization mechanism of MNA to NC

agreement with that of the previous report by Tang et al. (2016).

According to the abovementioned results and analysis and that of previous studies, the potential stability mechanism for MNA during NC/MNA (3 wt%) isothermal decomposition was proposed and summarized in Fig. 13. NO_x is generated when NC slowly decomposed under isothermal conditions. Then, MNA immediately absorbs NO_x to form the corresponding intermediate N-NO-MNA, which prevents NO_x from further catalyzing NC decomposition. As such, the thermal decomposition of NC is inhibited and its storage life is prolonged.

Conclusions

In summary, the interaction and mechanism of NC and MNA were investigated via the isothermal decomposition research method. Interestingly, a significant inflection point was found on the isothermal decomposition pressure–time curve of NC/MNA (3 wt%). The decomposition activation energy of NC/MNA (3 wt%) before the inflection point was 160.8 kJ mol^{-1}, which is higher than that of NC 145.6 kJ mol^{-1}. Thus, NC/MNA (3 wt%) thermal stability before the inflection point was better than that of pure NC. On the other hand, NC/MNA (3 wt%) decomposition activation energy after the inflection point was reduced to 140.7 kJ mol^{-1}, which was slightly lower than that of NC. In-depth studies have shown that as MNA/NC (3 wt%) thermal decomposition reached the inflection point, MNA was exhausted, resulting in a decreased

MNA/NC decomposition activation energy and thermal stability deterioration after the inflection point. NC/MNA (3 wt%) storage life was also calculated using Berthelot equation. The results showed NC storage life was significantly extended with stabilizer MNA addition. The effective storage life of NC at ambient temperature (298.15 K) can be extended from 10.57 to 24.9 years with the extent of reaction reaching 0.1% with 3 wt% MNA addition. The intermediate product of MNA and NC action was extracted and characterized, and the mechanism of the stabilizer MNA to NC involved the MNA absorption of NO_x to form N-NO-MNA.

References

Boers MN (2010) Lifetime prediction of EC, DPA, Akardite II and MNA stabilized triple base propellants, comparison of heat generation rate and stabilizer consumption. Propell Explos Pyrot 30:356–362

Chai H, Duan QL, Jiang L, Gong L, Chen HD, Sun JH (2019) Theoretical and experimental study on the effect of nitrogen content on the thermal characteristics of nitrocellulose under low heating rates. Cellulose 26:763–776

Chelouche S, Trache D, Tarchoun AF, Abdelaziz A, Khimeche K, Mezroua A (2019) Organic eutectic mixture as efficient

stabilizer for nitrocellulose: kinetic modeling and stability assessment. Thermochim Acta 673:78–91

Chu SJ (1994) Thermal analysis of explosive. Science press, Beijing

Cui G, Yoo JH, Yoo J, Lee SW, Nam H, Cha GS (2001) Differential thick-film amperometric glucose sensor with an enzyme-immobilized nitrocellulose membrane. Electroanalysis 13:224–228

Frys O, Bajerova P, Eisner A, Skladal J, Ventura K (2011) Utilization of new non-toxic substances as stabilizers for nitrocellulose-based propellants. Propell Explos Pyrot 36:347–355

Hu RZ, Gao SL, Zhao FQ (2008) Thermal analysis kinetics. Science press, Beijing

Krumlinde P, Ek S, Tunestal E, Hafstrand A (2017) Synthesis and characterization of novel stabilizers for nitrocellulose-based propellants. Propell Explos Pyrot 42:78–83

Lin CP, Li JS, Tseng JM, Mannan MS (2016) Thermal runaway reaction for highly exothermic material in safe storage temperature. J Loss Prevent Proc 40:259–265

Lindblom T (2002) Reactions in stabilizer and between stabilizer and nitrocellulose in propellants. Propell Explos Pyrot 27:197–208

Liu R, Zhou ZN, Yin YL, Zhang TL (2012) Dynamic vacuum stability test method and investigation on vacuum thermal decomposition of HMX and CL-20. Thermochim Acta 537:13–19

Luo LQ, Jin B, Xiao YY, Zhang QC, Chai ZH, Huang Q, Chu SJ, Peng RF (2019a) Study on the isothermal decomposition kinetics and mechanism of nitrocellulose. Polym Test 75:337–343

Luo LQ, Guo PL, Jin B, Xiao YY, Zhang QC, Chu SJ, Peng RF (2019b) An improved isothermal decomposition dynamics research instrument and its application in HMX/TNT/Al composite explosive. J Therm Anal Calorim. https://doi.org/10.1007/s10973-019-08554-5

Lussier LS, Bergeron E, Gagnon H (2006) Study of the daughter products of Akardite-II. Propell Explos Pyrot 31:253–262

Shekhar M (2011) Prediction and comparison of shelf life of solid rocket propellants using Arrhenius and Berthelot equations. Propell Explos Pyrot 36:356–359

Tai C, Zhang SD, Yin YG, Dai ZF, Li YB, Jiang GB, Cai Y, Huang CH, Shi JB (2018) Facile photoinduced generation of hydroxyl radical on a nitrocellulose nembrane surface and its application in the degradation of organic pollutants. ChemSusChem 11:843–847

Tan HM (2015) The chemistry and technology of solid rocket propellant. Beijing Institute of Technology Press, Beijing

Tang QF, Fan XZ, Li JZ, Bi FQ, Fu XL, Zhai LJ (2016) Experimental and theoretical studies on stability of new stabilizers for N-methyl-P-nitroaniline derivative in CMDB propellants. J Hazard Mater 327:187–196

Trache D, Khimeche K (2013a) Study on the influence of ageing on chemical and mechanical properties of N, N'-dimethyl-N, N'-diphenylcarbamide stabilized propellants. J Therm Anal Calorim 111:305–312

Trache D, Khimeche K (2013b) Study on the influence of ageing on thermal decomposition of double-base propellants and prediction of their in-use time. Fire Mater 37:328–336

Trache D, Tarchoun AF (2018a) Analytical methods for stability assessment of nitrate esters-based propellants. Crit Rev Anal Chem. https://doi.org/10.1080/10408347.2018.1540921

Trache D, Tarchoun AF (2018b) Stabilizers for nitrate ester-based energetic materials and their mechanism of action: a state-of-the-art review. J Mater Sci 53:100–123

Trache D, Khimeche K, Dahmani A (2013a) Solid–liquid phase equilibria for binary mixtures of propellant's stabilizers. J Therm Anal Calorim 112:215–222

Trache D, Khimeche K, Dahmani A (2013b) Study of (solid–liquid) phase equilibria for mixtures of energetic; material stabilizers and prediction for their subsequent performance. Int J Thermophys 34:226–239

Wilker S, Heeb G, Vogelsanger B, Jan P, Jan S (2007) Triphenylamine-a 'new' stabilizer for nitrocellulose based propellants-part I: chemical stability studies. Propell Explos Pyrot 32:135–148

Xiao YY, Bo J, Peng RF, Zhang QC, Liu QQ, Chu SJ, Guo ZC (2016) Thermal decomposition of CL-20 via a self-modified dynamic vacuum stability test. J Therm Anal Calorim 128:1833–1840

Zayed MA, Hassan MA (2010) Stability of non-isothermally treated double-base propellants containing different stabilizers in comparison with molecular orbital calculations. Propell Explos Pyrot 35:468–476

Zayed MA, Soliman AA, Hassan MA (2000) Evaluation of malonanilides as new stabilizers for double-base propellants. J Hazard Mater 73:237–244

Zayed MA, Mohamed AA, Hassan MA (2010) Stability studies of double-base propellants with centralite and malonanilide stabilizers using MO calculations in comparison to thermal studies. J Hazard Mater 179:453–461

Zayed MA, El-Begawy SEM, Hassan HES (2012) Enhancement of stabilizing properties of double-base propellants using nano-scale inorganic compounds. J Hazard Mater 227–228:274–279

Zayed MA, El-Begawy SEM, Hassan HES (2013) Mechanism study of stabilization of double-base propellants by using zeolite stabilizers (nano- and micro-clinoptilolite). Arab J Chem 10:573–581

Zhao X, Rui XT, Wang Y, Zhang RH (2018) A novel method for prediction of propellant shelf-life based on Arrhenius equation. Propell Explos Pyrot 43:348–354